Modelling superconducting nanowire single photon detectors in a waveguide cavity

Nicola A. Tyler,[*] Jorge Barreto, Gerardo E. Villarreal-Garcia, Damien Bonneau, Döndü Sahin, Jeremy L. O'Brien, and Mark G. Thompson

Centre for Quantum Photonics, University of Bristol, Bristol BS8 1TH, UK
[*]*Nicola.Tyler@bristol.ac.uk*

Abstract: In this work we report on a single photon detector system which offers near-unity detection efficiency using waveguide-coupled superconducting nanowires with lengths on the order of 1 μm. This is achieved by embedding the nanowires in a racetrack resonator where the interaction time with the photons trapped in the cavity is increased, thereby allowing for shorter nanowires. We expect this to lead to a higher fabrication yield as the amount of inhomogeneities decreases for shorter nanowires. Our simulations show a system with a 1 μm long superconducting nanowire single photon detector (SNSPD) operating at near-unity detection efficiency using design parameters that can be realistically achieved with conventional fabrication processes. The resonant cavity introduces spectral selectivity to the otherwise broad-band SNSPDs and the cavity induced timing jitter is shown to be insignificant for SNSPDs longer than 1 μm.

OCIS codes: (040.0040) Detectors; (140.4780) Optical resonators; (130.0130) Integrated optics; (130.7408) Wavelength filtering devices; (250.5300) Photonic integrated circuits; (230.5160) Photodetectors.

References and links

1. E. Knill, R. Laflamme, and G. J. Milburn, "A scheme for efficient quantum computation with linear optics," Nature **409**(6816), 46–52 (2001).
2. M. J. Collins, C. Xiong, I. H. Rey, T. D. Vo, J. He, S. Shahnia, C. Reardon, T. F. Krauss, M. J. Steel, A. S. Clark, and B. J. Eggleton, "Integrated spatial multiplexing of heralded single-photon sources," Nat. Commun. **4**, 2582 (2013).
3. D.-X. Xu, J. H. Schmid, G. T. Reed, G. Z. Mashanovich, D. J. Thomson, M. Nedeljkovic, X. Chen, D. Van Thourhout, S. Keyvaninia, and S. K. Selvaraj, "Silicon photonic integration platform—have we found the sweet spot?" IEEE J. Sel. Top. Quantum Electron. **20**(4), 8100217 (2014).
4. R. H. Hadfield, "Single-photon detectors for optical quantum information applications," Nat. Photonics **3**(12), 696–705 (2009).
5. C. Schuck, W. H. P. Pernice, and H. X. Tang, "Waveguide integrated low noise NbTiN nanowire single-photon detectors with milli-Hz dark count rate," Sci. Rep. **3**, 1893 (2013).
6. M. D. Eisaman, J. Fan, A. Migdall, and S. V. Polyakov, "Invited review article: Single-photon sources and detectors," Rev. Sci. Instrum. **82**(7), 071101 (2011).
7. S. Anders, M. G. Blamire, F.-I. Buchholz, D.-G. Crété, R. Cristiano, P. Febvre, L. Fritzsch, A. Herr, E. Il'ichev, J. Kohlmann, J. Kunert, H.-G. Meyer, J. Niemeyer, T. Ortlepp, H. Rogalla, T. Schurig, M. Siegel, R. Stolz, E. Tarte, H. J. M. ter Brake, H. Toepfer, J.-C. Villegier, A. M. Zagoskin, and A. B. Zorin, "European roadmap on superconductive electronics – status and perspectives," Physica C **470**(23-24), 2079–2126 (2010).
8. G. Gol'tsman, O. Okunev, G. Chulkova, A. Lipatov, A. Dzardanov, K. Smirnov, A. Semenov, B. Voronov, C. Williams, and R. Sobolewsk, "Fabrication and properties of an ultrafast NbN hot-electron single-photon detector," IEEE Trans. Appl. Supercond. **11**(1), 574–577 (2001).
9. A. J. Kerman, E. A. Dauler, J. K. W. Yang, K. M. Rosfjord, V. Anant, K. K. Berggren, G. N. Gol'tsman, and B. M. Voronov, "Constriction-limited detection efficiency of superconducting nanowire single-photon detectors," Appl. Phys. Lett. **90**(10), 101110 (2007).
10. K. M. Rosfjord, J. K. Yang, E. A. Dauler, A. J. Kerman, V. Anant, B. M. Voronov, G. N. Gol'tsman, and K. K. Berggren, "Nanowire single-photon detector with an integrated optical cavity and anti-reflection coating," Opt. Express **14**(2), 527–534 (2006).

#251338 Received 6 Oct 2015; revised 23 Jan 2016; accepted 25 Feb 2016; published 13 Apr 2016

11. X. Hu, E. A. Dauler, R. J. Molnar, and K. K. Berggren, "Superconducting nanowire single-photon detectors integrated with optical nano-antennae," Opt. Express **19**(1), 17–31 (2011).
12. P. Cavalier, J.-C. Villégier, P. Feautrier, C. Constancias, and A. Morand, "Light interference detection on-chip by integrated SNSPD counters," AIP Adv. **1**(4), 042120 (2011).
13. M. Hofherr, D. Rall, K. Ilin, M. Siegel, A. Semenov, H.-W. Hübers, and N. A. Gippius, "Intrinsic detection efficiency of superconducting nanowire single-photon detectors with different thicknesses," J. Appl. Phys. **108**(1), 014507 (2010).
14. F. Najafi, J. Mower, N. C. Harris, F. Bellei, A. Dane, C. Lee, X. Hu, P. Kharel, F. Marsili, S. Assefa, K. K. Berggren, and D. Englund, "On-chip detection of non-classical light by scalable integration of single-photon detectors," Nat. Commun. **6**, 5873 (2015).
15. G. N. Gol'tsman, K. Smirnov, P. Kouminov, B. Voronov, N. Kaurova, V. Drakinsky, J. Zhang, A. Verevkin, and R. Sobolewski, "Fabrication of nanostructured superconducting single-photon detectors," IEEE Trans. Appl. Supercond. **13**(2), 192–195 (2003).
16. C. Constancias, R. Espiau de Lamaëstr, O. Louveau, P. Cavalier, and J.-C. Villégier, "Patterning issues in superconducting nanowire single photon detector fabrication," J. Vac. Sci. Technol. B **25**(6), 2041 (2007).
17. R. Gaudio, K. P. M. op 't Hoog, Z. Zhou, D. Sahin, and A. Fiore, "Inhomogeneous critical current in nanowire superconducting single-photon detectors," Appl. Phys. Lett. **105**(22), 222602 (2014).
18. S. Miki, M. Fujiwara, M. Sasaki, and Z. Wang, "NbN superconducting single-photon detectors prepared on single-crystal MgO substrates," IEEE Trans. Appl. Supercond. **17**(2), 285–288 (2007).
19. F. Marsili, V. B. Verma, J. A. Stern, S. Harrington, A. E. Lita, T. Gerrits, I. Vayshenker, B. Baek, M. D. Shaw, R. P. Mirin, and S. W. Nam, "Detecting single infrared photons with 93% system efficiency," Nat. Photonics **7**(3), 210–214 (2013).
20. Y. P. Korneeva, M. Y. Mikhailov, Y. P. Pershin, N. N. Manova, A. V. Divochiy, Y. B. Vakhtomin, A. A. Korneev, K. V. Smirnov, A. G. Sivakov, A. Y. Devizenko, and G. N. Goltsman, "Superconducting single-photon detector made of MoSi film," Supercond. Sci. Technol. **27**(9), 095012 (2014).
21. V. B. Verma, B. Korzh, F. Bussières, R. D. Horansky, S. D. Dyer, A. E. Lita, I. Vayshenker, F. Marsili, M. D. Shaw, H. Zbinden, R. P. Mirin, and S. W. Nam, "High-efficiency superconducting nanowire single-photon detectors fabricated from MoSi thin-films," Opt. Express **23**(26), 33792–33801 (2015).
22. V. B. Verma, A. E. Lita, M. R. Vissers, F. Marsili, D. P. Pappas, R. P. Mirin, and S. W. Nam, "Superconducting nanowire single photon detectors fabricated from an amorphous $Mo_{0.75}Ge_{0.25}$ thin film," Appl. Phys. Lett. **105**(2), 022602 (2014).
23. E. A. Dauler, M. E. Grein, A. J. Kerman, F. Marsili, S. Miki, S. W. Nam, M. D. Shaw, H. Terai, V. B. Verma, and T. Yamashita, "Review of superconducting nanowire single-photon detector system design options and demonstrated performance," Opt. Eng. **53**(8), 081907 (2014).
24. J. P. Sprengers, A. Gaggero, D. Sahin, S. Jahanmirinejad, G. Frucci, F. Mattioli, R. Leoni, J. Beetz, M. Lermer, M. Kamp, S. Höfling, R. Sanjines, and A. Fiore, "Waveguide superconducting single-photon detectors for integrated quantum photonic circuits," Appl. Phys. Lett. **99**(18), 181110 (2011).
25. W. H. P. Pernice, C. Schuck, O. Minaeva, M. Li, G. N. Goltsman, A. V. Sergienko, and H. X. Tang, "High-speed and high-efficiency travelling wave single-photon detectors embedded in nanophotonic circuits," Nat. Commun. **3**, 1325 (2012).
26. D. Sahin, A. Gaggero, J.-W. Weber, I. Agafonov, M. A. Verheijen, F. Mattioli, J. Beetz, M. Kamp, S. Höfling, M. C. M. van de Sanden, R. Leoni, and A. Fiore, "Waveguide nanowire superconducting single-photon detectors fabricated on GaAs and the study of their optical properties," IEEE J. Sel. Top. Quantum Electron. **21**(2), 3800210 (2015).
27. K. M. Rosfjord, J. K. W. Yang, E. A. Dauler, A. J. Kerman, V. Anant, B. M. Voronov, G. N. Gol'tsman, and K. K. Berggren, "Nanowire single-photon detector with an integrated optical cavity and anti-reflection coating," Opt. Express **14**(2), 527–534 (2006).
28. M. K. Akhlaghi, E. Schelew, and J. F. Young, "Waveguide integrated superconducting single-photon detectors implemented as near-perfect absorbers of coherent radiation," Nat. Commun. **6**, 8233 (2015).
29. G. Abaeiani, V. Ahmadi, and K. Saghafi, "Design and analysis of resonant cavity enhanced-waveguide photodetectors for microwave photonics applications," IEEE Photonics Technol. Lett. **18**(15), 1597–1599 (2006).
30. J. Song, A. L. Eu-Jin, X. Luo, Y. Huang, X. Tu, L. Jia, Q. Fang, T.-Y. Liow, M. Yu, and G. Q. Lo, "Microring resonator photodetector for enhancement in L-band performance," Opt. Express **22**(22), 26976–26984 (2014).
31. Lumerical Solutions, Inc., *http://www.lumerical.com/tcad-products/mode/*.
32. V. Anant, A. J. Kerman, E. A. Dauler, J. K. W. Yang, K. M. Rosfjord, and K. K. Berggren, "Optical properties of superconducting nanowire single-photon detectors," Opt. Express **16**(14), 10750–10761 (2008).
33. A. Yariv, "Critical coupling and its control in optical waveguide-ring resonator systems," IEEE Photonics Technol. Lett. **14**(4), 483–485 (2002).
34. D. G. Rabus, *Integrated Ring Resonators* (Springer-Verlag, 2007).
35. M. Mesiya, *Contemporary Communication Systems* (McGraw-Hill Education, 2012).
36. E. Engin, D. Bonneau, C. M. Natarajan, A. S. Clark, M. G. Tanner, R. H. Hadfield, S. N. Dorenbos, V. Zwiller, K. Ohira, N. Suzuki, H. Yoshida, N. Iizuka, M. Ezaki, J. L. O'Brien, and M. G. Thompson, "Photon pair generation in a silicon micro-ring resonator with reverse bias enhancement," Opt. Express **21**(23), 27826–27834 (2013).
37. D. J. Lockwood and L. Pavesi, *Silicon Photonics II: Components and Integration* (Springer-Verlag, 2011).

#251338 Received 6 Oct 2015; revised 23 Jan 2016; accepted 25 Feb 2016; published 13 Apr 2016

38. A. J. Kerman, E. A. Dauler, W. E. Keicher, J. K. W. Yang, K. K. Berggren, G. Gol'tsman, and B. Voronov, "Kinetic-inductance-limited reset time of superconducting nanowire photon counters," Appl. Phys. Lett. **88**(11), 111116 (2006).
39. M. Ejrnaes, A. Casaburi, O. Quaranta, S. Marchetti, A. Gaggero, F. Mattioli, R. Leoni, S. Pagano, and R. Cristiano, "Characterization of parallel superconducting nanowire single photon detectors," Supercond. Sci. Technol. **22**(5), 055006 (2009).
40. Y. Ma, Y. Zhang, S. Yang, A. Novack, R. Ding, A. E.-J. Lim, G.-Q. Lo, T. Baehr-Jones, and M. Hochberg, "Ultralow loss single layer submicron silicon waveguide crossing for SOI optical interconnect," Opt. Express **21**(24), 29374–29382 (2013).
41. M. R. Watts, "Adiabatic microring resonators," Opt. Lett. **35**(19), 3231–3233 (2010).

1. Introduction

Single photon detectors (SPDs) are one of the fundamental building blocks of quantum photonic devices [1]. The performance of SPDs is especially critical if complex architectures such as multiplexed single-photon sources are considered [2], where detectors are used to herald single photons. Semiconductor materials, in particular silicon, are promising technological platforms for implementing complex quantum photonic devices. This is due to several factors including the high mode confinement achieved in waveguides, the existence of the fundamental building blocks for the generation and manipulation of light quanta, and the availability of a robust semiconductor industry capable of producing high-quality and high-yield devices [3]. The transmission in silicon waveguides peaks at infrared (IR) wavelengths, limiting the use of traditional semiconductor-based detectors. Superconducting nanowire SPDs (SNSPDs) are one of the best all-around candidates, offering high count rates along with low dark-count rates and low jitter [4–6]. SNSPDs are compatible with planar fabrication technologies, and can be made using niobium-based materials. These materials are well studied and already popular in the rapid single flux quantum (RSFQ) industry [7]. Niobium nitride (NbN) thin films are relatively easily accessible and have a superconducting transition temperature well above 4.2 K, allowing the use of both ^{4}Helium-based and cryogen-free cryostats.

Despite their many advantages, high-efficiency NbN SNSPDs are subject to very low fabrication yields [8–12]. The low yield of SNSPDs forces researchers to hand-pick the best devices from a batch [13]. In order to address this drawback, automated pick-and-place systems are required for high complexity circuits [14]. Detection efficiency of SNSPDs is correlated with length, such that nanowires of several hundreds of microns required to obtain high efficiencies [15]. However, with increasing SNSPD length the probability for defects increases. Thin NbN films suffer from imperfections [16,17] that reduce the critical current in nanowires and hence the SNSPD efficiency. These imperfections can be due to a number of reasons such as the lack of a monocrystalline structure arising from the deposition/growth process and patterning inhomogeneities. In addition, thinner NbN films present intrinsically lower transition temperatures further lowering critical current values [18], which makes the operation of the SNSPD more difficult. An alternative solution is the use of amorphous superconductors that are less prone to structural inhomogeneities, such as WSi [19], MoSi [20–22] and MoGe [22] yet at the cost of even lower operating temperatures and lower signal-to-noise ratios.

In commercial SNSPD systems, light is coupled from above onto a detector area consisting of a meander nanowire [23]. An alternative approach integrates SNSPDs in waveguide structures [24–26]. In such designs, the photon travels along a waveguide (WG) with an SNSPD directly above, leading to an increased interaction length of photon and nanowire. Since the absorption probability in such a system grows exponentially with length, near-unity detection efficiency can be achieved. Efficiencies above 90% have been reported with SNSPDs as short as 20 μm [25]. This nanowire length is significantly shorter than in the case of commercial top-coupled detectors. An additional advantage of WG coupled SNSPDs is the ability to implement SPDs in photonic circuits.

The implementation of detectors in optical cavities has been shown to improve efficiency for top-coupled devices by increasing the interaction time of the photon with the detector region [19,27]. Correspondingly, an optical cavity for WG-coupled SNSPDs increases the

#251338 Received 6 Oct 2015; revised 23 Jan 2016; accepted 25 Feb 2016; published 13 Apr 2016

interaction length, further decreasing the requirement for long nanowires. Recently, results on the integration of a WG coupled SNSPD inside a photonic-crystal cavity have been reported [28], demonstrating a highly efficient SNSPD with a length of only 8.5 μm. Furthermore, the use of a ring cavity has shown efficiency enhancement for photodiodes [29,30].

In this study, we propose a design that exhibits enhancement in both the detection efficiency and the fabrication yield of WG-coupled SNSPDs. This is achieved through the integration of a WG coupled SNSPD in a WG racetrack cavity. The cavity can be tuned to achieve resonance for any SNSPD size, maximizing the detection probability. This enables high detection efficiency for short SNSPDs. As discussed above, shorter nanowires are expected to suffer less from imperfections and hence present a higher fabrication yield. Furthermore, a shorter SNSPD provides a smaller area where possible dark counts could arise, and the dark count rate could therefore be strongly suppressed. In addition to the improvement of the detection probability, the configuration adds spectral dependence to the otherwise broad-band SNSPDs, allowing the design of integrated photonic spectrometers. In our study, we use an analytical model and support the results with numerical simulation data and find optimal as well as realistic design values.

2. Design and simulation model

This study examines an SNSPD in a cavity, the results are valid for any cavity type. A racetrack resonator was chosen as a representative cavity type, as it is common due to its fabrication ease, compatibility with standard photonic elements and the use of a single interface with the bus WG.

Our proposed cavity design can be seen in Fig. 1(a). It consists of a WG racetrack resonator containing a region with an integrated SNSPD and a bus waveguide. Light is coupled in and out of the resonator in the coupling region, interfering destructively in the output of the bus waveguide under critical coupling conditions and at resonance frequency. The detection efficiency reaches its peak value at critical coupling, where the losses within the cavity balance the coupling losses. In this case, single photons are trapped inside the cavity and remain there until either lost in the waveguide or absorbed by the nanowire, leading to near unity detection efficiency at resonance frequency.

We considered silicon-on-insulator (SOI) waveguides of 0.5 μm by 0.22 μm cross section, on a 1 μm thick SiO_2 slab. This waveguide is optimized for the fundamental transverse electric (TE) polarization mode. The refractive indices for silicon and SiO_2 were obtained from a commercial-grade simulator eigenmode solver and propagator [31]. The SNSPD consists of two 4.5 nm thick, 100 nm wide parallel NbN wires separated by 100 nm and centered on top of the waveguide. The dielectric constant of NbN was set to 5.23 + i5.82 based on [32] and was assumed constant within the studied wavelength range of 1545 nm – 1560 nm. The resonator was implemented as a racetrack cavity with a directional coupler in the coupling region. This allowed tuning of the transmissivity between 0 and 1 by changing the interaction length and the separation between the bus waveguide and the cavity. For all simulations the fundamental quasi-TE fundamental mode was considered.

#251338 Received 6 Oct 2015; revised 23 Jan 2016; accepted 25 Feb 2016; published 13 Apr 2016

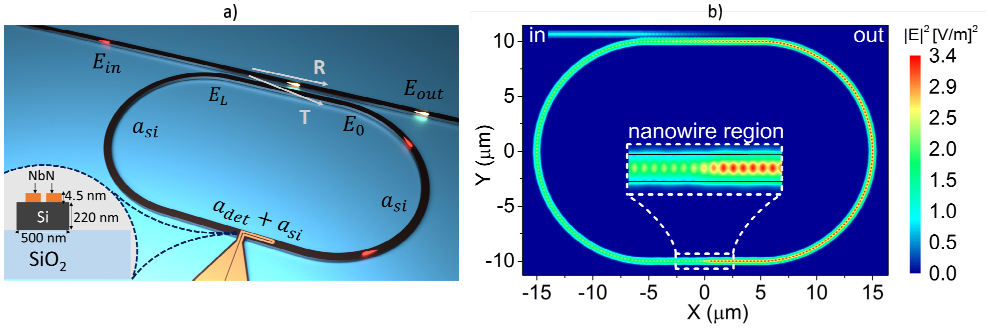

Fig. 1. Diagrams of an SNSPD inside a SOI waveguide racetrack resonator cavity. Four main regions are defined: the bus waveguide, the racetrack resonator, the coupling region between resonator and bus waveguide and the nanowire region inside the racetrack resonator. (a) Artistic depiction of the system. Light, E_{in}, is pumped and collected, E_{out}, in the bus waveguide. a: transmission coefficient per unit length, T: transmissivity, R: reflectivity, E_0: electric field inside racetrack at position 0, E_L: electric field inside racetrack at the end of one roundtrip at position L. The nanowire region is placed within the racetrack. (b) Simulated intensity distribution of a critically coupled cavity system with a 1.13 μm long SNSPD and a cavity length of 82.83 μm at 1553 nm, obtained using a commercial-grade simulator eigenmode solver and varFDTD propagator for the fundamental quasi-TE mode [31].

This structure was studied in two ways: analytically and numerically by looking at critical coupling conditions [33], and the results are compared. The SNSPD was modelled as two parallel, equally long nanowires which are not connected to each other or to electric pads. Loss due to reflections, caused by connecting the two nanowires and introducing a 90 degree bend towards the edge of the waveguide for electrical connections, was also studied. This was done by dividing the SNSPD into different areas of refractive indices and estimating resulting reflections. We found that the highest expected reflections are 0.004% which are negligible and therefore not included in the model.

To clarify terminology, the region with the two parallel nanowires that represent the SNSPD will hereafter be referred to as the nanowire region. Nanowire length will correspond to the length of the nanowire region. The system composed of the cavity and the SNSPD, will be referred to simply as the detector.

The analytical model has been implemented using MATLAB to estimate the evolution of the field intensity in the cavity. The model follows the schematic shown in Fig. 1(a), with the nanowire region lying inside the racetrack resonator. Light in the input port E_{in} reaches the coupling region of the resonator where a fraction stays in the bus waveguide after interfering with light exiting the cavity, E_{out}, and a fraction of the light goes into the racetrack, E_0. E_0 describes the light entering the resonator, and E_L the light after one roundtrip of length L where some light has been absorbed in the nanowire region and some lost due to scattering in the waveguide. The effect of the nanowires is modelled as a waveguide section with a corresponding effective refractive index. This takes into account the absorption of light and also the possible phase changes induced by the nanowires. Moreover, waveguide losses are included in the imaginary part of the refractive index.

The output field of the racetrack resonator for a single wavelength, λ, can be expressed [34] as:

$$E_{out}(\lambda) = \frac{r - \alpha e^{i\theta(\lambda)}}{1 - r\alpha e^{i\theta(\lambda)}} E_{in}(\lambda) \qquad (1)$$

where r represents the reflection coefficient of the coupling region, α the transmission coefficient inside the racetrack, and $\theta(\lambda)$ the accumulated phase for a photon with wavelength λ during one cavity cycle. The reflectivity r relates to the transmissivity of the

#251338 Received 6 Oct 2015; revised 23 Jan 2016; accepted 25 Feb 2016; published 13 Apr 2016

coupler as $T = 1 - r^2$, and the accumulated phase can be expressed as $\theta(\lambda) = 2\pi(n_{\text{eff, si}}(L - L_{nw}) + n_{\text{eff, nw}} L_{\text{nw}})/\lambda$. The two effective refractive indexes $n_{\text{eff, si}}$ and $n_{\text{eff, nw}}$ correspond to the fundamental modes of propagation in outside and inside the nanowire region, respectively. The transmission coefficient takes scattering loss in the waveguide along the racetrack length L into account, as well as loss due absorption in the nanowire region L_{nw}. It can be expressed as $\alpha = 10^{(a_{\text{det}} L_{\text{nw}} + a_{\text{si}} L)/20}$ with a_{nw} and a_{si} as the transmission coefficients in units of dB per unit length inside the nanowire region and the plain waveguide region. From Eq. (1) we derive that E_{out} reaches its minimum when $r = \alpha e^{i\theta(\lambda)L}$.

The total power absorbed inside the racetrack is calculated by comparing the input and output power in the bus waveguide. In this model, once light is coupled into the cavity, it can only be absorbed in the nanowire region or lost due to scattering in the waveguide, leading to a total absorption probability by the detector of

$$P(\lambda)_{\text{abs, total}} = 1 - \left(\frac{E_{\text{out}}(\lambda)}{E_{\text{in}}(\lambda)} \right)^2 = 1 - \left(\frac{r - \alpha e^{i\theta(\lambda)}}{1 - r\alpha e^{i\theta(\lambda)}} \right)^2 \tag{2}$$

An estimation of the power absorbed into the nanowires can be obtained from this by subtracting the contribution from waveguide scattering. This is done by calculating the fraction F_{nw} of light absorbed by the nanowires inside the racetrack:

$$F_{nw} = (1 - \eta_{\text{si, beg}})\eta_{\text{nw}} \sum_{n=0}^{\infty} (1 - \eta_{\text{nw}})^n (1 - \eta_{si})^n = \frac{(1 - \eta_{\text{si, beg}})\eta_{\text{nw}}}{1 - (1 - \eta_{\text{nw}})(1 - \eta_{\text{si}})} \tag{3}$$

where $\eta_{\text{si, beg}}$ is the scattering probability in the silicon waveguide from the beginning of the resonator until the beginning of the nanowire section, and η_{nw} and η_{si} are the absorption probabilities into the nanowires of the nanowire region and the silicon waveguide for one round trip, respectively.

Absorption probabilities of the detector into the nanowires are obtained by multiplying $P(\lambda)_{\text{abs, total}}$ with the correction factor for waveguide scattering F_{nw}. We assume 100% internal quantum efficiency for the nanowires and therefore directly relate the absorption probability into the nanowires to the detection efficiency η for a given continuous wave (CW) wavelength λ_{CW} as

$$\eta = P(\lambda_{\text{CW}})_{\text{abs, total}} F_{\text{nw}} = \left(1 - \left(\frac{r - \alpha e^{i\theta(\lambda_{\text{CW}})}}{1 - r\alpha e^{i\theta(\lambda_{\text{CW}})}} \right)^2 \right) \frac{(1 - \eta_{\text{si, beg}})\eta_{\text{det}}}{1 - (1 - \eta_{\text{det}})(1 - \eta_{\text{si}})} \tag{4}$$

As mentioned above, the efficiency η is maximized when the light leaving the cavity E_{out} is minimized. This occurs when the system is critically coupled ($r = \alpha$) and phase-matched ($e^{i\theta(\lambda_{\text{CW}})L} = 1$). Equation (4) simplifies in these cases and is represented by η_{pm} for a phase matched detector, by η_{cc} for the efficiency of a critically coupled detector, and $\eta_{\text{pm, cc}}$ for a detector which is phase matched as well as critically coupled and calculated using following equations

$$\eta_{\text{pm}} = \left(1 - \left(\frac{r - \alpha}{1 - r\alpha} \right)^2 \right) \frac{(1 - \eta_{\text{si, beg}})\eta_{\text{det}}}{1 - (1 - \eta_{\text{det}})(1 - \eta_{\text{si}})} \tag{5a}$$

#251338 Received 6 Oct 2015; revised 23 Jan 2016; accepted 25 Feb 2016; published 13 Apr 2016

$$\eta_{cc} = \left(1 - \left(\frac{r(1-e^{i\theta(\lambda_{CW})})}{1-r^2 e^{i\theta(\lambda_{CW})}}\right)^2\right)\frac{(1-\eta_{si,\,beg})\eta_{det}}{1-(1-\eta_{det})(1-\eta_{si})} \tag{5b}$$

$$\eta_{pm,\,cc} = \frac{(1-\eta_{si,\,beg})\eta_{det}}{1-(1-\eta_{det})(1-\eta_{si})} \tag{5c}$$

In addition to CW input, pulses with Gaussian frequency distribution are considered as input fields E_{in}. Since the system is linear and time invariant, we can model the output intensity by using the transfer function describing the system in frequency domain with a specific input pulse [35]. In our study, the input field E_{in} is defined as a Gaussian distribution and the output pulse is calculated using Eq. (1) for a set of frequencies independently. The energy stored in a light pulse can be calculated by integrating the square of the electric field in frequency f leading to an expression for an effective pulse efficiency of:

$$\eta_{pulse} = 1 - \left(\frac{\int E_{out}(f)^2\,df}{\int E_{in}(f)^2\,df}\right) \tag{6}$$

Single-photon sources based on ring resonators have been shown to generate single photons routinely around 1.55 μm with a full-width at half-maximum (FWHM) in wavelength of 0.1 nm [36], which is one of the parameters in our simulations for pulse input sources.

Five main parameters are investigated in this study: nanowire length L_{nw}, cavity length L, transmissivity in the coupling region of the resonator *T*, photon wavelength λ and the FWHM of the photon pulse in the frequency domain. The first three parameters are design and fabrication related. The transmissivity can be obtained from the characteristics of the directional coupler in the case of a racetrack resonator. The other two parameters (λ and the FWHM) are related to the photon and depend both on the generation mechanism and on the propagation of the photon prior to reaching the detector.

In order to confirm the analytical results, the detector was simulated numerically using the variational FDTD solver of a commercial-grade simulator eigenmode solver and FDTD propagator [31]. The amount of light in the output bus waveguide was monitored for different nanowire lengths inside a racetrack resonator. A racetrack length of just below 83 μm was chosen for the ring-cavity. The length of 82.83 μm is the result of two 10 μm bend-radius semicircles and 10 μm long straight waveguide sections, which is a reasonably standard geometry for the fabrication process of a low loss resonator. The cavity has a resonance frequency at 1553 nm. The separation of the bus waveguide and straight section of the resonator is 160 nm, resulting in a simulated transmissivity value for the directional coupler of 0.31. An example of a field intensity plot with a nanowire length of 1.13 μm is shown in Fig. 1(b).

The variational FDTD simulations are presented only for an 82.83 μm long cavity and nanowire lengths between 0.1 μm and 5 μm. Other cavity systems between 19 μm and 192 μm in size and nanowire lengths of 0.05 μm and 35 μm are investigated using the analytical model. The studied wavelength range includes 1545 nm – 1560 nm. CW sources as well as Gaussian pulses of up to 1 nm FWHM are modelled for waveguide losses between −0.5 dB/cm and −4 dB/cm. The results of this analysis are presented in section 3.

3. Results

The effective refractive indices used in the analytical model were calculated using an eigenmode solver [31] to be $n_{eff} = 2.42$ and $n_{eff} = 2.41 + i\,0.04$ outside and inside the nanowire region, respectively. Various values for scattering losses in the waveguide were investigated, and −2 dB/cm is used as a default value if not mentioned otherwise.

#251338 Received 6 Oct 2015; revised 23 Jan 2016; accepted 25 Feb 2016; published 13 Apr 2016

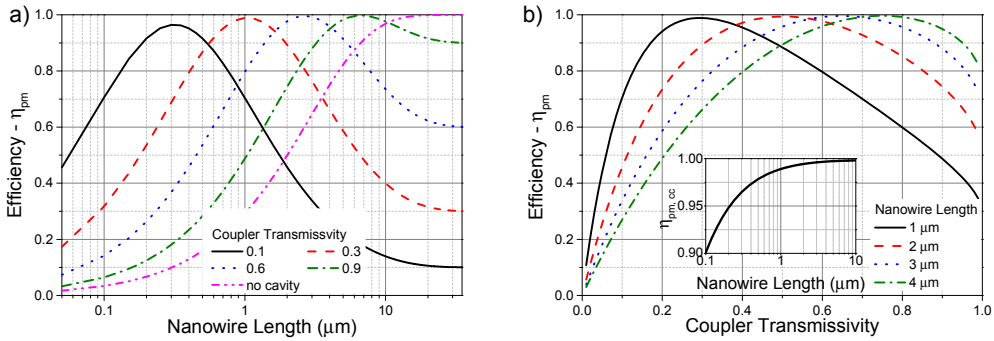

Fig. 2. (a) Change in detector efficiency with nanowire length. The curves represent different cavity types with transmissivity values in the coupling region between 0.1 (black line) and 0.9 (green dash-dot line), and for a nanowire region without the cavity (magenta dash-dot-dot line). (b) Efficiency as a function of coupler transmissivity. Four systems with nanowire lengths between 1 and 4 μm (black line – green dash-dot line) are shown. Inset: Efficiencies at matching versus nanowire length with coupler transmissivities optimized at each point for critical coupling.

Calculation parameters: 83 μm racetrack length, phase matched around 1553 nm, CW input, −2 dB/cm waveguide loss Fig. 2(a) shows the detection efficiency calculated using Eq. (5a) for different nanowire lengths considering racetrack resonator systems with several transmissivity values in the coupler region. The curves are shown in comparison to a nanowire region on a straight waveguide with the same dimensions but without a cavity. Detection efficiencies close to unity can be achieved with shorter nanowire lengths than for a nanowire region on a straight waveguide without cavity. These high efficiencies can be reached due to the increased interaction time between the photon and the nanowires. For a small coupler transmissivity, a short nanowire length (L_{nw} < 1 μm) is sufficient to obtain near unity efficiency. For each nanowire length there is a certain optimum coupler transmissivity as shown in Fig. 2(b) which was also calculated using Eq. (5a). Detection efficiencies under critical coupling and phase matching conditions increase with nanowire length according to Eq. (5c) as shown in the inset of Fig. 2(b). This is because a longer nanowire region leads to proportionally less scattering in the waveguide and therefore higher detection efficiencies.

A short nanowire region is desirable as defects scale with length [17], therefore SNSPDs with short nanowires promise a higher fabrication yield. In addition, short SNSPDs are expected to show reduced dark counts, as a smaller nanowire area decreases the probability of triggering false counts.

We will now investigate the dependence on other parameters of the system, such as the wavelength of the input photon, its spectral width, the size of the cavity and waveguide loss.

#251338 Received 6 Oct 2015; revised 23 Jan 2016; accepted 25 Feb 2016; published 13 Apr 2016

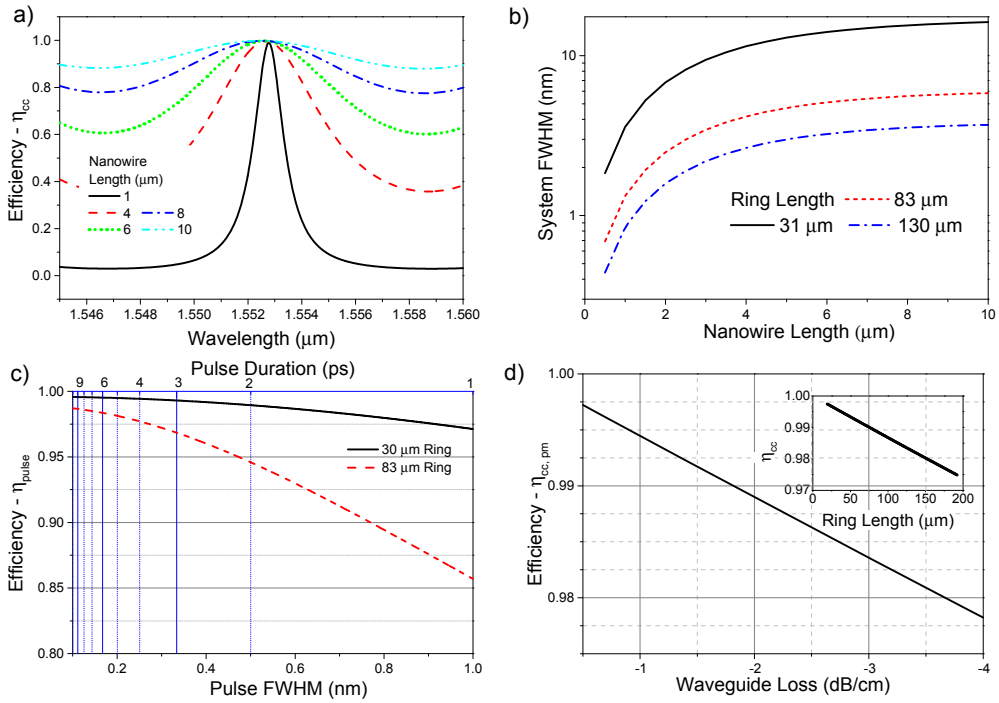

Fig. 3. (a) Efficiency response versus wavelength for various nanowire lengths between 1 μm and 10 μm. The response is dependent on wavelength due to the presence of a cavity. Racetrack size: 83 μm. (b) FWHM of the detection efficiency response to wavelength versus nanowire length for different cavity sizes. Calculation parameters for (a) and (b): critically coupled, CW input and -2 dB/cm waveguide loss. (c) Efficiency response to different input pulses for 30 μm and 83 μm racetracks. Calculation parameters: 1 μm nanowire length, center wavelength around 1550 nm, critically coupled, -2 dB/cm waveguide loss. (d) Maximum efficiency at critical coupling versus waveguide loss (main image, 83 μm racetrack length) and racetrack length (inset: –2 dB/cm waveguide loss). Calculation parameters: 1 μm nanowire length, CW input and phase matched around 1550 nm.

Figure 3(a) shows the frequency response of the detection efficiency for CW input at critical coupling which was calculated using Eq. (5b). The shape of the detection efficiency is clearly determined by the resonance frequency of the cavity, with sharper peaks for shorter nanowires. This makes our detector attractive as building block for single photon sensitive spectrometers. The width of the efficiency curve and the minimum efficiency at a wavelength off resonance depend on nanowire length. Shorter nanowires show a narrow wavelength response, while the bandwidth increases with longer nanowires due to the effect of the cavity being shadowed by increased loss. The FWHM of the wavelength response versus nanowire length at critical coupling for different racetrack sizes was studied using equation Eq. (5b) and is shown in Fig. 3(b). The FWHM decreases for larger cavity sizes and shorter nanowire lengths. In the case of an 83 μm ring without nanowires but with loss solely due to scattering, the FWHM of the resonance spectrum is 1.5 pm.

So far the input light has been considered to be CW, however the behavior of a single photon can be modelled more accurately when considering pulses. We therefore studied the response of the detector to pulses with a Gaussian frequency distribution with a FWHM of up to 1 nm and central wavelength around 1550 nm. These results are shown in Fig. 3(c) for a critically coupled system with a 1 μm long nanowire using Eq. (6). The efficiency drops with increasing FWHM of the pulse width. The drop in efficiency is more pronounced for longer rings, which is in accordance with the previously shown narrower frequency response for larger rings. As mentioned above, 0.1 nm is an achievable pulse width for a single photon

#251338 Received 6 Oct 2015; revised 23 Jan 2016; accepted 25 Feb 2016; published 13 Apr 2016

[36]. For a 0.1 nm FWHM, the efficiency drops by only 0.4% and 1.3% for 30 µm or 83 µm long cavities, respectively, and even less for a FWHM below 100 pm.

Scattering of light inside the waveguide decreases the ultimate detection efficiency. This was calculated under phase matched and critically coupled conditions according to Eq. (5c) and is shown in Fig. 3(d) for an 83 µm long racetrack with a 1 µm nanowire region. Increasing the racetrack size leads to a drop in nanowire absorption as the interaction length between waveguide and photon increases, leading to more loss due to scattering. An increase in loss due to a decrease of bend radius can also be modelled in the same way. However, the results show that even for a relatively high waveguide loss of up to −4 dB/cm, detection efficiencies close to 98% can still be reached.

Trapping the light in a cavity could affect the timing resolution of the detector negatively. If the nanowire length is very short, the photon resides longer in the cavity before being absorbed, which can lead to a decrease in timing resolution. The jitter is a common measure for the timing resolution. It is often defined as the FWHM of the variation in time difference between photon arrival and photon detection. To estimate the effect on the extrinsic jitter due to the cavity, we assume that the system is critically coupled and that the photon is trapped in the cavity before detection. The extrinsic jitter was calculated considering the time between photon arrival in the cavity and its detection (according to the number of measurements within the FWHM for a normally distributed set of measurements) with an effective group index of 4.2 and a cavity length of 30 µm, 83µm and 130 µm. The results for different nanowire lengths are presented in Fig. 4(a). We can see that the extrinsic jitter increases for racetrack cavities with shorter nanowires, however for nanowire lengths of around 1 µm and above, the time is significantly smaller than typical intrinsic jitter values, which can be as short as 18 ps [25].

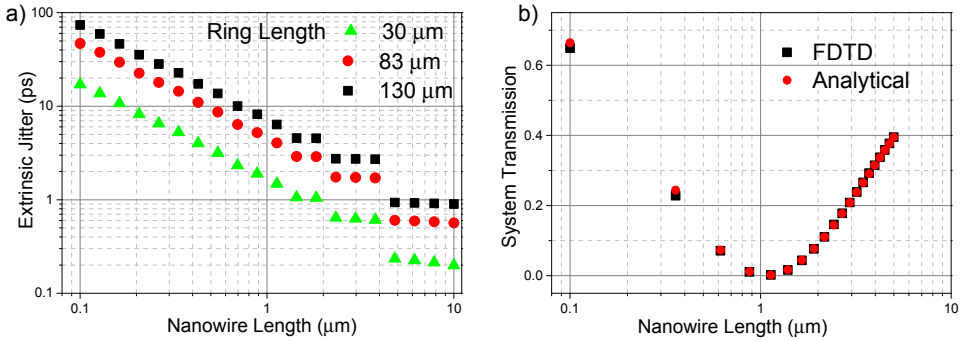

Fig. 4. (a) Time between photon arrival in the cavity and 75.8% absorption by the nanowires as a measure of the extrinsic jitter for several racetrack lengths. (b) Data comparison of varFDTD simulations and analytical calculations. System transmission for different lengths of integrated nanowire. Transmissivity at beam splitter: 0.31, racetrack length: 83 µm, CW at 1553 nm.

Finally, a racetrack resonator of 83 µm in length was simulated numerically for CW light using a varFDTD solver [31]. The simulations were performed for several nanowire lengths between 0.1 µm and 5 µm. For each simulated nanowire length the power in the output waveguide was recorded, which is a measure for the transmission of the system. The results are shown in Fig. 4(b) in comparison to the analytical simulations using Eq. (2) which are in high agreement. The system transmission varies with the nanowire length inside the cavity. At a nanowire length of 1.13 µm the transmission is at a minimum of 0.24%. Around this point critical coupling takes place and the detection probability is maximized. The simulated intensity distribution for this point is shown in Fig. 1(b).

4. Discussion

From the results, we conclude that small racetrack sizes give higher efficiencies with a broader wavelength response. Detectors with small racetrack cavities are less sensitive to

#251338 Received 6 Oct 2015; revised 23 Jan 2016; accepted 25 Feb 2016; published 13 Apr 2016

frequency variance, more tolerant to the spectral width of the incoming photon and experience less contribution to loss from waveguide scattering. All of the aforementioned reasons make small racetrack cavities favorable for high performance and broad band detectors. In reality the size of the cavity is limited by the choice of fabrication technology. In order to achieve adequate transmission in bent structures, the bend radius should not be smaller than 4 μm [37]. This sets a minimum size for the racetrack at > 25 μm, plus potential straight sections of the racetrack. In addition, we conclude that the nanowires should not be much shorter than 1 μm, as systems with very short nanowires are more sensitive to small changes in nanowire length, e.g. due to fabrication tolerances, as shown in Fig. 2(a). Furthermore, decreasing the nanowire length below 1 μm can have a negative effect on the extrinsic timing jitter, while systems with nanowires of 1 μm or larger lead to an increase of only 2 ps in jitter value for 30 μm long racetracks or 8 ps in case of 130 μm racetrack length.

Table 1 shows case studies of different designs and their performance in efficiency, frequency response and jitter. The design with 130 μm racetrack length and 1 μm nanowire length is an example for a detector which is highly wavelength selective. This design is highly narrow-band as shown in Fig. 3(b), and could be used for spectrometer purposes due to a small FWHM in wavelength response of 0.85 nm. The efficiency at resonance wavelength is 98% for a 50 pm input pulse. At a wavelength detuned from the resonance however, the detector is only responsive in 3% of the cases. Instead, a racetrack length of 82.83 μm is a good compromise, offering high efficiency for pulses for slightly larger pulses, as well as wavelength selectivity. The efficiency for a 1 μm nanowire region and a 100 pm input pulse is 98.7% with 1.3 nm FWHM in wavelength response. Inserting a longer nanowire region decreases wavelength selectivity and therefore 99.8% efficiency can be reached with a 10 μm nanowire region and 0.1 nm pulses. The use of even smaller racetracks and larger nanowires further broadens the wavelength response. For 30 μm a racetrack and a 10 μm nanowire region, pulses as broad as 10 nm result in high efficiencies of 99%. The wavelength response is extremely broad with a FWHM of more than 16 nm. This system is very close to unity efficiency, 99.9%, when used with short pulses of 100 pm. Moreover, a very short nanowire length of 0.2 μm can reach efficiencies of up to 97.7% at resonance when placed in a small racetrack of 30 μm and is highly wavelength sensitive with only 0.2% efficiency off resonance and a narrow FWHM of 0.8 nm in wavelength response. The small cavity size also ensures that the extrinsic jitter of 8.7 ps is not too high, despite the short length of the nanowire region. Depending on the requirement, all designs come with their own benefits regarding resonance bandwidth and nanowire length. In all cases, the extrinsic jitter due to the cavity presence is short, 10 μm nanowire systems add cavity jitters of less than 1 ps.

Table 1. Example designs with performance parameters in efficiency, frequency response and jitter. R_L: racetrack length, L_{nw}: nanowire length, $FWHM_p$: FWHM of input pulse, $\eta_{cc,pm}$: efficiency at resonance, $\eta_{cc,or}$: efficiency off-resonance, λ_r: resonance wavelength, $\lambda_{s\text{-}FWHM}$: FWHM of wavelength response, J: jitter. All data were simulated at critical coupling and for a waveguide loss of −2 dB/cm.

R_L (μm)	L_{nw} (μm)	$FWHM_p$ (nm)	$\eta_{cc,pm}$ (%)	$\eta_{cc,of}$ (%)	λ_r (nm)	$\lambda_{s\text{-}FWHM}$ (nm)	J (ps)
130.1	1	0.05	98.2	3.0	1550.0	0.9	8.2
82.8	1	0.1	98.7	3.0	1552.8	1.3	5.2
82.8	10	0.1	99.8	87.9	1552.4	5.8	0.7
30.1	10	0.1	99.9	87.8	1549.0	16.3	0.2
30.1	10	10.0	99.0	88.6	1549.0	16.6	0.2
30.1	0.2	0.1	97.4	0.2	1550.0	0.8	8.7

In terms of the electrical characteristics of very short SNSPDs, it is known that the kinetic inductance scales with nanowire length and is therefore expected to be small for short SNSPDs. A small inductance leads to a short SNSPD recovery time [38] which in general is an advantage when high speed operation is desired. However, short recovery times can result in latching issues, a problem that can be addressed with the addition of an inductance in series [39].

#251338 Received 6 Oct 2015; revised 23 Jan 2016; accepted 25 Feb 2016; published 13 Apr 2016

Finally, it should to be mentioned that additional loss inside the cavity will be introduced due to the electrical connections that have to be made to the SNSPD. These connections can be achieved via a bridge structure to the silicon waveguide. Recent results have shown losses for waveguide crossing as low as −0.03 dB [40], which is not expected to decrease the detection efficiency significantly. The design can be further optimized by placing the SNSPD on an adiabatically widened bend region [41], minimizing the losses by increasing the effective mode size and hence it's overlap with the bridging structure. Electrical connections can then be made via a cross to the inside of the racetrack, which is expected to reduce the loss even further.

5. Conclusions

We have presented simulation results detailing the performance of SNSPDs integrated within racetrack resonator cavities. The results illustrate the potential of cavity-coupled photon detectors, in particular waveguide-coupled superconducting nanowire single-photon detectors. Our simulations show that it is possible to achieve efficiency values very close to unity with nanowires as short as 1 μm. This promises to address the yield problem observed in long NbN SNSPDs. In addition, the spectral characteristics of this type of detector match the response of the cavity they are embedded in, allowing for custom-designed spectrometers. Our results agree with the experimental results in [28], suggesting that by embedding SNSPDs in a cavity it is possible to reach high-efficiency detection with sub-10 μm nanowires. The racetrack resonator suggested in this work benefits from ease of fabrication and compatibility with silicon-on-insulator photonics, as well as even further reduction of nanowire length.

Acknowledgments

The authors are grateful to Daryl Beggs, Gary Sinclair, Joshua Silverstone and Allison Rubenok for useful discussions. This work was supported by Engineering and Physical Sciences Research Council (EPSRC), Defence Science and Technology Laboratory (DSTL), European Research Council (ERC), CONACYT (CVU: 409778), the University of Bristol, the Marie Curie Actions within the Seventh Framework Programme for Research of the European Commission, under the ITN PICQUE, Grant No. 608062, FP7 Action: Beyond the Barriers of Optical Integration (BBOI) and the Centre for Nanoscience and Quantum Information (NSQI). J.L.O'B. acknowledges a Royal Society Wolfson Merit Award and a Royal Academy of Engineering Chair in Emerging Technologies.

#251338 Received 6 Oct 2015; revised 23 Jan 2016; accepted 25 Feb 2016; published 13 Apr 2016